Similarities between mode III crack growth patterns and strike-slip faults

T. Cambonie, Y. Klinger, Veronique Lazarus

PHILOSOPHICAL TRANSACTIONS A

rsta.royalsocietypublishing.org

Research

Article submitted to journal

Subject Areas:
Plate tectonics, mechanical engineering, mechanics

Keywords:
fracture patterns, strike-slip faults, mode III

Author for correspondence:
V. Lazarus
e-mail: veronique.lazarus@ensta.fr

Similarities between mode III crack growth patterns and strike-slip faults

T. Cambonie[1], Y. Klinger[2] and V. Lazarus[3]

[1]Univ Lyon, ENTPE, LTDS UMR CNRS 5513, 3 rue Maurice Audin, 69518 Vaulx en Velin Cedex, France.
[2]Institut de Physique du Globe de Paris, Sorbonne Paris Cite, Universite Paris Diderot, UMR 7154 CNRS, Paris, France
[3]IMSIA, ENSTA ParisTech, CNRS, CEA, EDF, Université Paris-Saclay, 828 bd des Maréchaux, 91762 Palaiseau cedex, France

Why are strike slip faults not perfectly linear but made of successive segments? Are they reminiscence of the fracture of an initially sound crust by the bottom-up propagation of a crack subjected to mode III loading? The plausibility of this newly proposed scenario will be investigated here through model experiments and some theoretical explanations in the framework of brittle fracture.

In Nature strike-slip faults usually do not appear to be linear features. Although assessing detailed geometry of strike-slip faults at the kilometric scale can prove to be difficult, earthquakes offer a unique opportunity to get insights on how faults might be structured along strike. Indeed, when large strike-slip earthquakes occur, they generate ground surface ruptures that can be up to several hundreds of kilometer long [1,2]. Based on field observations and seismological results, it has been suggested that these surface ruptures, beyond the inherent variability related to local site effects, are actually most often organized in a series of consecutive fault segments connected by relay zones, either fault bends or step-overs [3] (fig. 1a). According to observations, the average length of individual segments seems to be rather constant, between 15 km and 20 km, and this independently of local tectonic and geological conditions (see fig. 8). Understanding (i) why strike-slip faults would be structured in such a way along strike, and (ii) what might control their geometry and in particular the segment length, are keys to address questions related to seismic hazard mitigation.

THE ROYAL SOCIETY PUBLISHING

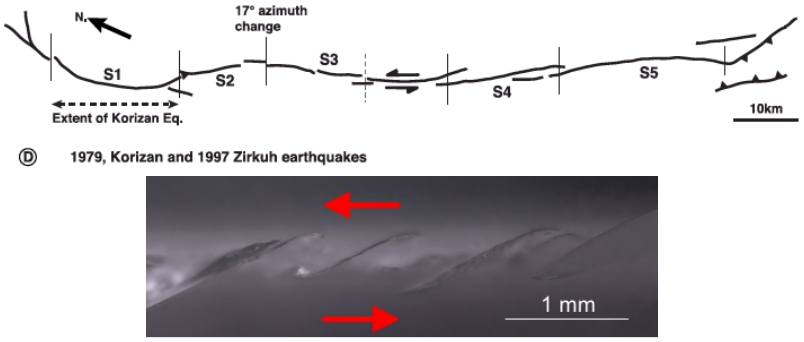

Figure 1. (a) Why does a strike-fault appear as a succession of smaller segments? [3] (b) Are they reminiscence of the segmentation of an initially sound crust by the bottom-up propagation of a crack subjected to mode III loading? [4]

If strike-slip faults would be segmented with segments of similar length, such structure could be implemented in earthquake simulators to limit the number of earthquake scenarios to be tested [5] and could have some control on potential earthquake magnitude to be expected. The task is however not straightforward since the geometry of the fault, as we can observe it nowadays, is the combination of possible pre-existing geological structures superimposed with a more recent fault structure that has evolved through a multitude of earthquake cycles since its emplacement. In the next sections, following the suggestion that crack/fault geometry presents some continuity through scales [6], we propose in (§1) to examine through a model experiment the formation of a segmented pattern (fig. 1b) by crack propagation when mode III shear loading is applied [7–9]. From there, we formulate a plausible scenario for the formation of the strike-slip fault segments (§2) where fault segments, as they can be observed today, would be the reminiscence of the initial fault pattern formed during the fracture of the pristine Earth crust, through the bottom-up propagation of a basal crack subjected to mode III loading related to far-field tectonic boundary conditions.

1. Crack propagation in presence of mode III

When a crack is loaded in presence of anti-plane shear (tear) loading (mode III), segmentation of the crack front occurs during propagation [7–9]. This phenomenom is quite universal from the millimeter [9] to the kilometer scales [10], in many types of materials going from metals [11], to polymers [9,12], glass [7], cheese [13], soft matter [14] and rocks [10]. Fracture experiments realized in plexiglas [9] at the lab scale can thus be considered to be representative of what happens in the earth crust at larger scale. The main advantage of using plexiglass is that *in-situ* observations of the segment formation are possible by transparency, although in Nature, only the trace of their formation, in its final state (potentially after many successive seismic events) and at the top of the crustal layer, can be studied. Here, in addition to former fatigue (performed under cyclic loading) experiments [4,9,15], some new experiments broken abruptly under increasing loading until fracture are also presented. Fatigue and these supplementary outputs, together with some theoretical results of interest for our purpose [16–18], are outlined below.

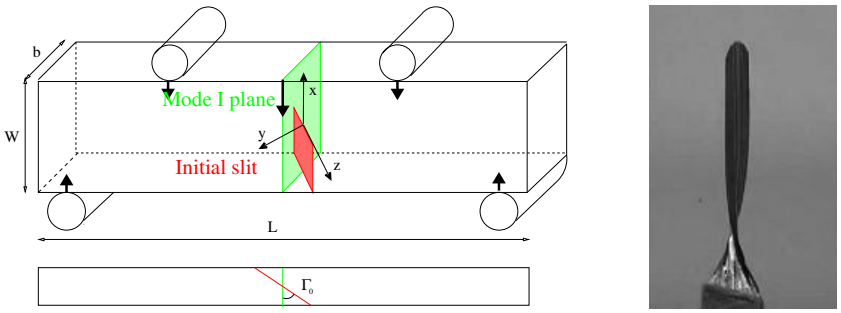

Figure 2. Left: experimental bending setup; To introduce some tear loading, the initial slit (in red) is inclined in reference to the mode I plane (in green). Right: picture taken by transparency from the left side of the specimen; the crack surfaces appear in dark; the initial crack front (at the bottom of the picture, width 100 mm) twists to ultimately reach the mode I plane.

(a) Bending experiments

Experiments are carried out using *cast* plexiglass[1] beams and a traditional four point bending setup (Fig. 2). An initial crack is manufactured by micro-milling and further sharpened by pushing a razor blade inside [4]. To introduce some amount of mode III, the crack is tilted with an angle Γ_0 from the mode I central plane of symmetry (that corresponds to $\Gamma_0 = 0$) [9,12,19]. When Γ_0 increases, the amount of shear mode III increases. We consider two ways of propagating the crack: (i) either progressive propagation under cyclic loading (fatigue) to observe in-situ the segment formation or (ii) abrupt propagation once the brittle fracture threshold is reached, leading directly to the breaking of the sample into two pieces (brittle fracture). The beams size is $L = 50$ mm, $W = 10$ mm, $b = 10$ mm. In brittle fracture, a loading velocity $V = 0.1$ mm.s^{-1} has been selected to break all the samples. In fatigue, the loading parameters of the 5 Hz cyclic loading $F_0 \pm \Delta F$ had to be adjusted for each sample to keep the loading per unit crack length constant. F_0 and ΔF increase with Γ_0 and range from 180 ± 160 N for $\Gamma_0 = 5^0$ to 340 ± 300 N for $\Gamma_0 = 45^0$. More informations on the sample and experiment preparation can be found in [9] and the supplemental material of [4].

In fatigue, in-situ observations can simply be made by stopping the loading cycles. At the macroscopic scale of the sample (fig. 2), the crack front twists during the propagation to ultimately reach the mode I plane [9]. On a smaller scale (fig. 3), the initial crack front splits into an array of very small daughter cracks, that are shaped as tilted facets rotated toward the shear free direction, and that coarse during propagation. Fig. 3a-c, which correspond to the same Γ_0 experiment at different stages of the propagation, highlight that the coarsening occurs by the progressive coalescence (or merging) of the facets during in-depth propagation. This process induces an increase of the spacing between the facets with the propagation length. This coarsening process is also clearly visible on the post-mortem fracture surfaces in fig. 3e, where the distance between the merging zones (appearing in white) increases in the propagation direction (from bottom to top).

Under monotonic loading, the crack abruptly propagates once the brittle fracture threshold is reached. It is not possible to follow the facets formation in-situ, but observations can be made on the broken samples. For $\Gamma_0 \leq 15$ degrees, the final fracture surfaces are similar to the ones obtained in fatigue (fig. 3e), suggesting a similar formation process. For $\Gamma_0 > 15$ degrees, the complete segmentation of the full crack front becomes difficult to achieve; the fracture of the specimen in two pieces generally results from the nucleation, in discontinuity with the initial

[1]obtained by casting the polymer. This fabrication process garanties that the material is isotropic, in contrary to plexiglass obtained by *extrusion* which is in general anisotropic.

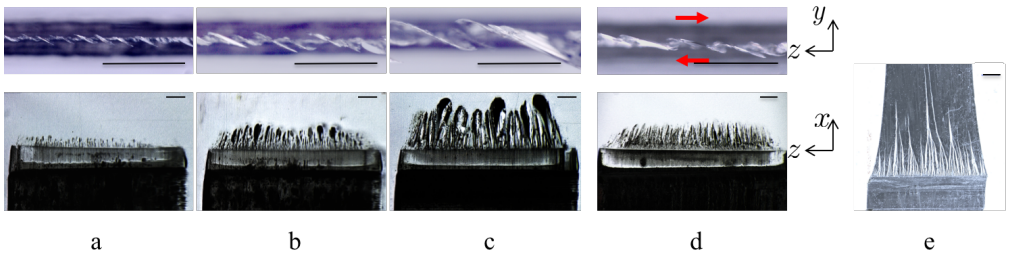

Figure 3. (a-d) In-situ numerical microscope images of partially broken samples. Each column corresponds to one sample, the first row being a top view and the second row being a front view as indicated by cartesians axes defined in fig. 2. $\Gamma_0 = 30^0$ in (a)-(c) and $\Gamma_o = 15^0$ in (d). In the front views, the initial slit and the facets appear in black. In the bottom views, the initial larger slit is dark and the facets appear in white; the red arrows corresponds to the direction of the mode III shear loading in reference of the initial slit. (e) Post-mortem front views of the fracture surfaces corresponding to $\Gamma_0 = 15^0$. The coarsening zones appear in white. The bar scale is 1 mm long in all images

front, of a unique fracture in the mode I plane. In the sequel, experiments corresponding to this last case will not be considered further.

(b) Results on the length scale S and the orientation θ

Whether under cyclic loading or monotonic loading (for $\Gamma_0 \leq 15^0$), the fracture pattern can be characterized by the evolution with the propagation length a of (i) the spacing S between the facets and (ii) the tilt angle θ with the initial slit (fig. 4).

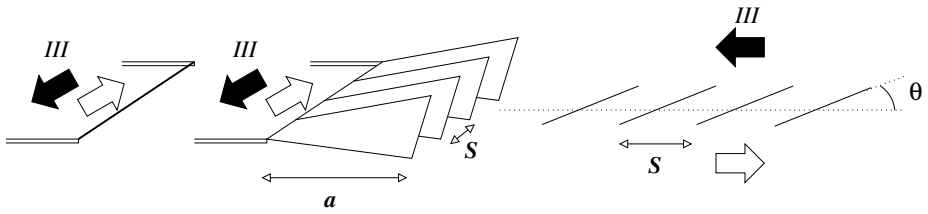

Figure 4. Schematic view of the segmented pattern and definitions of S, θ and a.

To get quantitative informations on the patterns, three-dimensional maps of post-mortem fracture surfaces are obtained using a profilometer. The tilt angle $\theta(a)$, the spacing $S(a)$ are then extracted line by line for the successive values of a, as detailed in [15]. Figure 5 is representative of their evolution under both cyclic and monotonic loading. The successive coalescence of the facets (as observed qualitatively on fig. 3), induces a nearly linear increase of $S(a)$, which can be quantified by the coarsening rate $\beta \equiv \frac{\mathrm{d}S}{\mathrm{d}a}$. The tilt angle $\theta(a)$ increases from the initial flat position of the slit $\theta(a=0)=0$ to a maximum $\theta_{\max}$ before it decreases. This decrease is linked to the decrease of the amount of mode III induced by the overall twisting of the front (fig. 2), as demonstrated in [15].

Figure 6 gives the evolution of β and of $\theta_{\max}$ with Γ_0. Several observations can be made: (i) the angle $\theta_{\max}$ and the coarsening rate β increase with Γ_0, that is with the amount of mode III; (ii) the angle $\theta_{\max}$ and the coarsening rate β are nearly the same, although slightly higher in fatigue than for brittle fracture; (iii) as mentioned previously, for $\Gamma_0 > 15^0$, facets are not likely to occur in brittle fracture, this is why there are no 'black points' above this value.

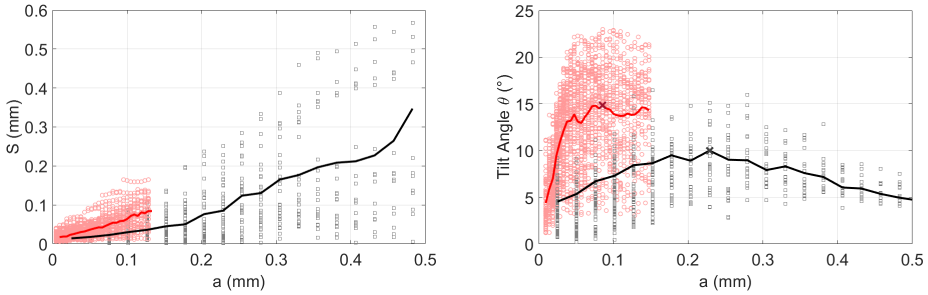

Figure 5. Evolution of the spacing S and the tilt angle θ during propagation ($\Gamma_0 = 10^0$). For a given propagation length a, each point corresponds to the length between two facets (Left) or to the rotation angle of one of them (Right); the line corresponds to their mean value. The red color corresponds to fatigue, the black one to brittle fracture.

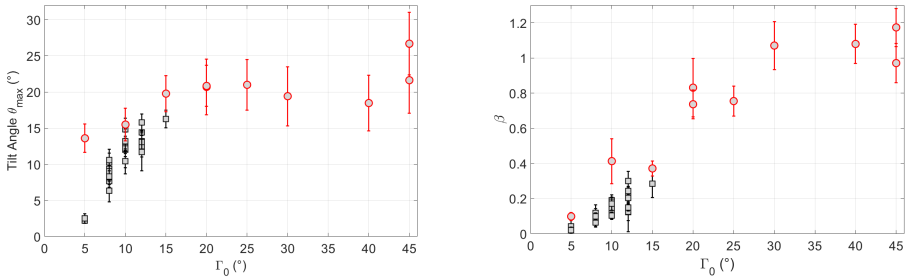

Figure 6. Influence of Γ_0 on the maximum tilt angle $\theta_{\max}$ and on the coarsening rate $\beta \equiv \frac{\mathrm{d}S}{\mathrm{d}a}$. β is obtained by linear regression for $a < 150\mu$m. Each point corresponds to one experiment. For the maximum tilt angle $\theta_{\max}$, the error bars corresponds to the standard deviation of the facet angle distribution at the peak location (cf Fig. 5). For the coarsening rate β, the error bars corresponds to the upper and lower bounds of the 95 % confidence interval of the linear regression. The ○ correspond to fatigue, the □ to brittle fracture.

(c) Theoretical insights

In the framework of linear elastic fracture, the crack advance is described using the **S**tress **I**ntensity **F**actors (abbreviated SIF) K_I, K_{II}, K_{III} and the energy release rate G [20]. Under a cyclic loading, the crack advance at each loading cycle depends in a complex way (not precisely known as for now in mixed mode) on the amplitude of the SIFs [21]. Under an increasing loading, the crack does not advance until the elastic energy released by the crack propagation balances the fracture toughness G_c; in other words, the brittle fracture threshold is given by $G = G_c$. The crack propagation direction, whether under cyclic or monotonic loading [22], is given by the **P**rinciple of **L**ocal **S**ymmetry (PLS) which states that $K_{II} = 0$ [23]. In 3D, these criterions ($G = G_c$, $K_{II} = 0$) has to be applied point by point along the crack front. Phase-field methods are a way to find the crack path satisfying these conditions [24].

Consider the ideal case of a planar crack with a straight crack front submitted to an uniform mixed mode I + III (therefore in the absence of mode II); A trivial solution is an uniform and coplanar advance of the front (fig. 7Left). But besides this trivial solution, it has been shown by linear stability analysis that a deformed helical solution exists above a K_{III}/K_I threshold [16,25]. We have also shown [4] by phase-field simulations, that this instability is subcritical and that the bifurcated solution takes the form of crack front segmentation and facet coarsening (fig. 7Right),

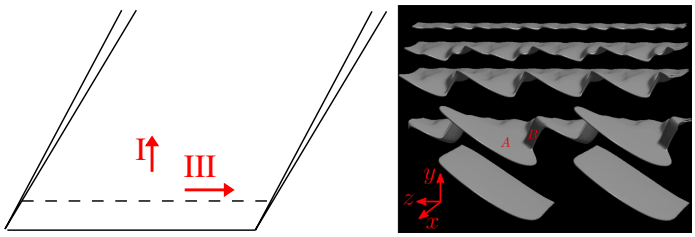

Figure 7. A planar crack with a straight front loaded uniformly in mode I+III. Left: trivial solution, that is straight and coplanar crack propagation (the dotted and full lines are resp. the initial and final positions of the crack front). Right: bifurcated solution, corresponding to the segmentation of the initial crack front into facets and their further coalescence (courtesy A. Karma).

in agreement with the experiments. In other words, it means that in practice, the formation of segments can be initiated as soon as some amount of mode III is present, provided that the large enough defects exist to initiate the instability.

Concerning the segmentation patterns, the facets are rotated toward the direction of the shear free direction [18]. The tilt angles θ are lower than the shear free direction [4,26]. This can be attributed to the mutual shielding of the loading by adjacent facets [27]. Indeed, the values of θ are in agreement with the phase-field simulations which inherently take these interactions into account. Concerning β, only a qualitative agreement on the increase of β with Γ_0 could be found; some ingredients are still missing. Furthermore, it is possible to show using a multiscale cohesive zone model [17], that (i) under a constant loading the spacing S has to scale linearly with a to get a sustained propagation in the form of disconnected tilted facets, (ii) the slope $\beta = S/a$ increases with K_{III}/K_I. Further work is under progress to get precisely the value of β as a function of the parameters involved in the problem, that is material constants (G_c, ν) and the local loading of the tips given by the stress intensity factors. But this task is complex and beyond the scope of this paper.

2. Plausible scenario for the strike-slip fault formation

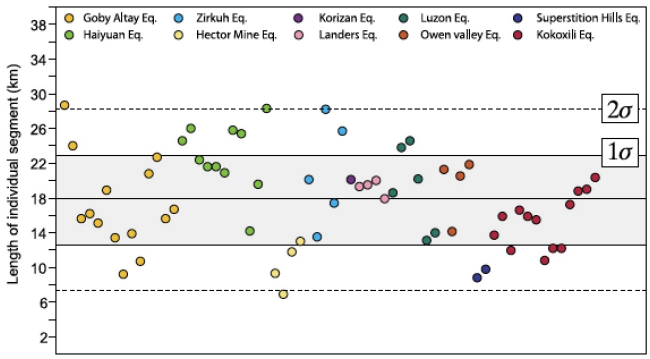

Figure 8. Segments observed in strike-slip faults. The length of the segments measured on different faults is $S \sim 17.5$ km at any location. Since the thickness T of the crust is almost constant, it was suggested that $S \propto T$ [3].

Large continental strike-slip faults affect the entire lithosphere, although the brittle part of the crust is usually only limited to the upper 15 to 20 top kilometers, where earthquakes occur. These large continental faults propagate to accommodate large-scale plate-tectonic boundary conditions [28]. They are driven by the shear stress located at the base of the crust. Although this can be considered a rough first-order approximation, a propagating strike-slip fault can be envisioned as a fracture propagating in a pristine piece of crust under basal traction, following the direction of a small circle that defines the rotation of two rigid crustal blocks at the surface of spherical Earth. Hence, at the base of the crust, when the fracture initiates, it is expected to have a direction parallel to the shear direction. When the fracture grows upward toward the free surface, it has been shown that the direction of the fracture changes for the fracture to become in a shear-free direction. Although it is beyond the scope of this work, studying geometries of exhumed strike-slip faults to compare them with the direction of stress at the time these structures were active could be enlightening in this regard. Available outcrops with enough relevant data might, however, prove to be very limited, making this further work difficult.

Since defects are unavoidable in particular in the Earth crust, the subcritical instability described in §1 is likely to appear. Hence, when breaking the full crust, a basal crack loaded in mode III, (i) will form tilted facets rotated toward the shear free direction; (ii) as the fracture propagates upward the distance S between consecutive facets will increasing; (iii) there will be a linear relation between S and the propagation direction, so that when emerging at the surface S will scale with the plate thickness T.

In the case of the Lithosphere, the thickness of the brittle part of the crust only differs in a minor way between the different continents and on average it is considered to be 15 km to 20 km thick for any continent. Thus, transposing the results from the model experiment to the emplacement of strike-slip faults, if the thickness of the brittle crust is, at first order, similar anywhere, the distance S between successive ruptured sections when they reach the ground surface should also be similar for any strike-slip fault, about 15 km to 20 km (fig. 8). It is worth to notice that this yields $S/T \sim 1$ which is close to the values of β obtained experimentally for large enough Γ_0 values (fig. 6), giving some additional arguments for the scenario. Although only very few large strike-slip earthquake ruptures have been documented in oceanic-crust setting, the 1998, M7.9, event in Antartica, which ruptured through an oceanic crust, shows a rupture segmentation shorter than segmentation observed for continental earthquakes, consistent with a thinner oceanic brittle crust [3]. Despite the well defined mean ruled by fracture mechanics principles at the continuum scale, some natural variability will arise depending on places (fig. 8) due to (i) the facet initiation ruled by defect scattering and (ii) further propagation perturbed by heterogeneities.

In an idealized pristine crust, these upward propagating fractures correspond to Riedel cracks [29] that form first, with some obliquity relative to the direction of shear. In real Earth, though, the true direction of the Riedel cracks will be a combination of the theoretical predicted angle and of the effect of preexisting geological structures, introducing some heterogeneity, and likely anisotropy that could partly guide the growth of the fracture. Later, as the fault structure evolves to accommodate the shear traction applied at the base of the crust, these Riedel cracks get connected by a coalescent network of through going cracks that will eventually becomes the main fault. While the system is evolving towards this more mature stage, the initial Riedel cracks might be partly dismantled to eventually only persist as geometric discontinuities in-between more linear sections of the fault. In Nature, these discontinuities would be interpreted as relay zones, such as fault bend or step-over. Hence, strike-slip fault as we can see them today, have often evolved significantly from such initial simple geometry and what can be seen, mostly during earthquakes rupture, is the remains of such blueprint, which is preserved through constant length of fault segments separated by relay zones.

3. Conclusion

Facet formation under shear mode III has been reported since a long time [7–9]. We review here some recent theoretical, numerical and experimental results showing that their formation can be predicted in the framework of linear elastic fracture mechanics [4]: The trivial straight

and planar solution (without any segments) of the classical criterions (Griffith and Principle of Local Symmetry) is unlikely to appear since any defect or material heterogeneity may initiate a subcritical instability corresponding to the apparition of facets, that coalesce during propagation. Using self-similarity arguments [17], the spacing can be argued to scale with the propagation distance, the theoretical determination of the proportionality constant being devoted to further work. Here, this constant is quantified experimentally (fig. 6) and noticed to be close to the values observed in faults (fig. 8). In addition to the fatigue experiments of [4], we also report new experiments performed by abrupt fracture of the specimens, that show no significant changes on the in-fine morphologies. But, the main novelty of the paper is to transpose these results from the fracture mechanics to the geophysics/mechanics communities in order to show the plausibility of the new scenario proposed herein for the strike-slip fault segmentation, as the reminiscence of the fracture of an initially sound crust by the bottom-up propagation of a crack subjected to mode III loading.

Data Accessibility. Insert details of how to access any supporting data here.

Authors' Contributions. The fatigue experiments in fatigue were performed by TC during his postdoctoral study under the supervision of VL. YK, field expert in strike-slip faults, was the principal investigator of the ANR project GeoSMEC which funded this work. He is the initiator of the idea to explain the segment length by shear experiments. VL, expert in fracture mechanics, coordinated the study and drafted the manuscript. All authors read and approved the manuscript.

Funding. These work was funded by ANR GeoSmec (ANR-12-BS06-0016).

Acknowledgements. The authors would like to thank A. Karma, J.B. Leblond, C. Ravi-Chandar and coworkers for their contributions in the theoretical and numerical parts and D. Bonamy, L. Hattali, V. Doquet, V. De Greef, L. Auffray, R. Pidoux for their help in the experimental parts.

References

1. Y. Klinger, X. Xu, P. Tapponnier, J. Van der Woerd, C. Laserre, and G. King.
High-resolution satellite imagery mapping of the surface rupture and slip distribution of the Mw 7.8, november 14, 2001 Kokoxili earthquake (Kunlun fault, Northern Tibet, China).
Bull. Seis. Soc. Am., 95(5):1970–1987, 2005.
2. J.H. Choi, Y. Klinger, M. Ferry, J.F. Ritz, R. Kurtz, M. Rizza, L. Bollinger, B. Davaasambuu, N. Tsend-Ayush, and S. Demberel.
Geologic inheritance and earthquake rupture processes : The 1905 M $\geq$ 8 Tsetserleg-Bulnay strike-slip earthquake sequence, Mongolia.
J. Geophys. Res. : Solid Earth, 123, 2018.
3. Y. Klinger.
Relation between continental strike-slip earthquake segmentation and thickness of the crust.
Journal of Geophysical Research, 115(B07306), 2010.
4. C.-H. Chen, T. Cambonie, V. Lazarus, M. Nicoli, A. J. Pons, and A. Karma.
Crack Front Segmentation and Facet Coarsening in Mixed-Mode Fracture.
Physical Review Letters, 115(26):265503, 2015.
5. E. H. Field, T. H. Jordan, M. T. Page, K. R. Milner, B. E. Shaw, T. E. Dawson, G. P. Biasi, T. Parsons, J. L. Hardebeck, and A. J. Michael.
A synoptic view of the third uniform California earthquake rupture forecast (UCERF3).
Seismological Research Letters,, 88(5):1259–1267, 2017.
6. T. Candela, F. Renard, Y. Klinger, K. Mair, J. Schmittbuhl, and E. E. Brodsky.
Roughness of fault surfaces over nine decades of length scales.
J. Geophys. Res., 117(B08409), 2012.
7. E. Sommer.
Formation of fracture 'lances' in glass.
Engineering Fracture Mechanics, 1:539–546, 1969.
8. D. Hull.
The effect of mixed-mode I/III on crack evolution in brittle solids.
International Journal of Fracture, 70(1):59–79, 1995.

9. V. Lazarus, F.-G. Buchholz, M. Fulland, and J. Wiebesiek.
Comparison of predictions by mode II or mode III criteria on crack front twisting in three or four point bending experiments.
International Journal of Fracture, 153:141–151, 2008.
10. D. D. Pollard, P. Segall, and P. T. Delaney.
Formation and interpretation of dilatant echelon cracks.
Geological Society of America Bulletin, 93:1291–1303, 1982.
11. A. Eberlein, H.A. Richard, and G. Kullmer.
Facet formation at the crack front under combined crack opening and anti-plane shear loading.
Engineering Fracture Mechanics, 174:21 – 29, 2017.
Special Issue on Multiaxial Fracture 2016.
12. Bisen Lin, M. Mear, and K. Ravi-Chandar.
Criterion for initiation of cracks under mixed-mode I+III loading.
International Journal of Fracture, 165:175–188, 2010.
10.1007/s10704-010-9476-7.
13. R. Goldstein and N. Osipenko.
Successive development of the structure of a fracture near the front of a longitudinal shear crack.
Doklady Physics, 57:281–284, 2012.
10.1134/S1028335812070087.
14. O. Ronsin, C. Caroli, and T. Baumberger.
Crack front échelon instability in mixed mode fracture of a strongly nonlinear elastic solid.
EPL (Europhysics Letters), 105(3):34001, February 2014.
15. T. Cambonie and V. Lazarus.
Quantification of the crack fragmentation resulting from mode I+III loading.
Procedia Materials Science, 3:1816–1821, 2014.
16. J.B. Leblond, A. Karma, and V. Lazarus.
Theoretical analysis of crack front instability in mode I+III.
Journal of the mechanics and physics of Solids, 59:1872–1887, 2011.
17. J.-B. Leblond, V. Lazarus, and A. Karma.
Multiscale cohesive zone model for propagation of segmented crack fronts in mode I+III fracture.
International Journal of Fracture (Special Invited Article Celebrating IJF at 50), 191(1):167–189, February 2015.
18. K. H. Pham and K. Ravi-Chandar.
Further examination of the criterion for crack initiation under mixed-mode I+III loading.
International Journal of Fracture, 189(2):121–138, 2014.
19. F.-G. Buchholz, A. Chergui, and H. A. Richard.
Fracture analyses and experimental results of crack growth under general mixed mode loading conditions.
Engineering Fracture Mechanics, 71(4-6):455–468, 2004.
20. K. B. Broberg.
Cracks and fracture.
Academic Press, 1999.
21. T. Bonniot, V. Doquet, and S. H. Mai.
Mixed mode II and III fatigue crack growth in a rail steel.
International journal of fatigue, 2018.
22. W. Linnig.
Some aspects of the prediction of fatigue crack paths.
In H. P. Rossmanith and K. J. Miller, editors, *Mixed-Mode Fatigue and Fracture. ESIS 14*, pages 201–215. Mechanical Engineering Publications, 1993.
23. R. V. Goldstein and R. L. Salganik.
Brittle fracture of solids with arbitrary cracks.
International Journal of Fracture, 10:507–523, 1974.
24. Vincent Hakim and Alain Karma.
Laws of crack motion and phase-field models of fracture.
Journal of the Mechanics and Physics of Solids, 57(2):342 – 368, 2009.

25. Antonio J. Pons and Alain Karma.
Helical crack-front instability in mixed-mode fracture.
Nature, 464:85–89, 2010.
26. M. L. Cooke and D. D. Pollard.
Fracture propagation paths under mixed mode loading within rectangular blocks of polymethyl methacrylate.
Journal of Geophysical Research, 101(B2):3387–3400, 1996.
27. J.-B. Leblond and J. Frelat.
Development of fracture facets from a crack loaded in mode I+III: solution and application of a model 2D problem.
Journal of the Mechanics and Physics of Solids, 64:133–153, 2014.
28. P. Tapponnier, G. Peltzer, A. Ledain, R. Armijo, and P. Cobbold.
Propagating extrusion tectonics in Asia – New insights from simple experiments with plasticine.
Geology, 10(611-616), 1982.
29. J. S. Tchalenko and N. N. Ambraseys.
Structural analysis of the Dasht-e Bayaz (Iran) earthquake fractures.
Geological Society of America Bulletin, 81(1):41–60, 1970.